Optical localization transition in a dual-periodical phase-modulated synthetic photonic lattice

Siwei Tang, Chunlei Shang, Chengzhen Lu, Xiaolei Sun, Yangjian Cai,* Yuanmei Gao,† and Zengrun Wen‡
Center of Light Manipulations and Applications and Shandong Provincial Key Laboratory of Optics and Photonic Devices, Shandong Normal University, Jinan 250014, China
and School of Physics and Electronics, Shandong Normal University, Jinan 250014, China

(Received 7 March 2022; accepted 19 January 2023; published 6 February 2023)

We investigated optical localization and vibration in a synthetic photonic lattice (SPL) with two-phase modulators driven by different periodic voltages. By altering the periods of phase modulation, the induced phase circumfluences, band structure, and transmission behaviors of light in the SPL are studied. A transition from discrete diffraction to weak localization was observed in a small modulation period with equal modulation periodicities. For large modulation periods, the band structure exhibits a density distribution and the optical field delocalizes and vibrates. In contrast, strong localization occurs near the initial incident location with some moiré modulation periods of phases that correspond to a flat-band structure. This study reveals the effect of dual-periodic phase modulation on pulse propagation in discrete systems.

DOI: 10.1103/PhysRevA.107.023505

I. INTRODUCTION

Localized light fields have attracted intensive interest in theoretical and experimental studies over the past few decades [1,2]. Optical localization can enhance the interaction between light and matter, improve the performance of lasers, and realize lasing with high modulation rates and low thresholds [3–5]. Research on optical localization has successfully demonstrated some basic phenomena with potential application value, thereby attracting broad attention in the scientific community [3]. Owing to the strong impact of diffraction and dispersion in the process of light propagation, the broadening effect of light waves has been introduced [6,7]. Several studies showed that the dispersion can be mitigated by introducing randomness and balanced by nonlinearity, which led to the Anderson localization and solitons, respectively [8–11]. In addition, defects and dynamic modulation also enable the existence of optical localization in photonic lattices [6,12–17].

The recent booming research field of moiré photonics provides a new and efficient way to achieve optical localization [18–21]. Moiré lattices are formed by overlapping two identical or similar periodic structures with a twist angle or tuned lattice frequency, which adds a new adjustable dimension for optical localization. Compared with the previous system, the localized mode provided by the moiré lattice is simpler and more flexible without the need for a strong refractive index contrast, special structure design, and strong laser power. The moiré lattice is a prominent example of how to explore new wave phenomena caused by purely geometric properties. The dispersion of such systems, for example, flat energy band, band-gap engineering, and localization-to-delocalization of light, can be modulated by changing the angle between the two child components [18,19,22–24]. In addition, optical localization can be realized by frequency detuning and nonlinearity [7,20,25]. In a one-dimensional system, the moiré lattice can be obtained by superimposing two Bragg gratings with different periods, whereas Bragg gratings with the same period form a so-called non-moiré lattice [21,26]. The localization effect occurs when the beam is incident on the node of the moiré lattice, on the other hand, the optical Zitterbewegung effect is achieved when the initial beam is injected on the peak [21].

The concept of a synthetic dimension has recently come to light as a feasible path for exploring higher-dimensional physics in lower-dimensional systems by simulating spatial coordinates using nonspatial degrees of freedom. In contrast to photonic crystals, synthetic dimensions possess intrinsic flexibility, low cost, and high operability, without the need for complex processing technology [27–30]. Among different synthetic systems, synthetic photonic lattices (SPL) are composed of two mutually coupled fiber rings that have been successfully utilized to simulate optical behaviors in discretized structures [27], quantum communication, quantum computing, and so on [31–33]. A unique property of a one-dimensional SPL is the discrete expansion of light transmission in two axes owing to the time-multiplexing technique [34–36]. Several explorations of surrounding optical localization were proposed. For example, Anderson localization in SPL was achieved by phase disorder and static random coupling disorder [1,34]. Bloch oscillations in Hermitian and non-Hermitian (global or local $\mathcal{PT}$) systems were investigated by adding a gradient phase along the time axis [37]. In addition, the localization caused by the defect is in $\mathcal{PT}$-symmetric lattice [38], the localization is achieved by an effective gauge-field interface [39] and optical funneling is achieved by introducing the non-Hermitian topology [40]. In the above research, the SPL model is used to simulate and

*yangjiancai@suda.edu.cn
†gaoyuanmei@sdnu.edu.cn
‡wenzengrun@163.com

apply a variety of optical localization phenomena. Compared to general waveguide arrays, this model is discrete in time and position, which endows the SPL with the ability to verify new theories or explore new optical transmission behaviors [41,42]. Therefore, it is worth studying the energy band variation and transmission behavior of light in SPL with moiré modulation.

In this study, a model of SPL with two-phase modulations governed by two cosine functions with different periods was established. With the adjustment of the period of the double-phase modulations, the combination of the two phases induces non-moiré and moiré phase accumulations along the space (transverse) axis. We analyzed the relationship between phase accumulation and band structure and studied the localization-to-delocalization transitions that exist in both non-moiré and moiré phase accumulations. The localization distribution with respect to the two modulation periods was investigated using statistical methods. In contrast to Anderson localization created by fiber rings with random modulation [34], the localized transmission trajectory in this study is deterministic and repeatable. In addition, the localization-to-vibration transition of SPL with a large periodic modulation was also simulated and analyzed. We further confirm that the localization intensity is not only related to the number of flat bands but also the band gaps.

II. FUNDAMENTAL MODEL OF SPL WITH DUAL-PERIODIC PHASE MODULATIONS

Figure 1(a) shows the time-multiplexing scheme, which is formed by two coupled fiber loops with a length difference ΔL. When a periodic pulse train is launched into a longer or shorter loop, two new pulse sequences are generated in each loop after it passes through the coupler. The pulse returns to the coupler in the long and short loops with an average time of T and a relative delay time of ΔT. Because the lengths of the two loops are different, the pulse train returns to the coupler after a round trip in the long loop is delayed compared with that in the short loop, and then the two pulse trains are split again by the coupler. As the number of round trips increases, a pulse train over time is eventually generated, which is similar to the beam dynamics in the optical mesh lattice. Interestingly, the arrival time of each pulse at the coupler can be reinterpreted as an index of position along the synthetic spatial dimension, expressed as $t = mT + n\Delta T$, where m is the number of times each pulse enters the coupler (discrete-time coordinates) and n is the number of times the pulse passes through the long loop more than the short loop (space-like coordinates). As the light propagates, m increases to record subsequent increases in the number of round trips, whereas n can increase or decrease depending on which loop the light travels. Whereafter, m can be reinterpreted as a continuously increasing number of discrete time steps, where n is a discrete position index. We relate the average round-trip times through the coupler to the discrete-time step m and the discrete arrival time to the relative position of the pulse in the sequence n, leading to the equivalent mesh lattice in the time domain described in Fig. 1(b). The equivalent $(1 + 1)$ lattice model was used several times in the field of optics. In Fig. 1(b), we indicate the corresponding phase on the grid diagram. We

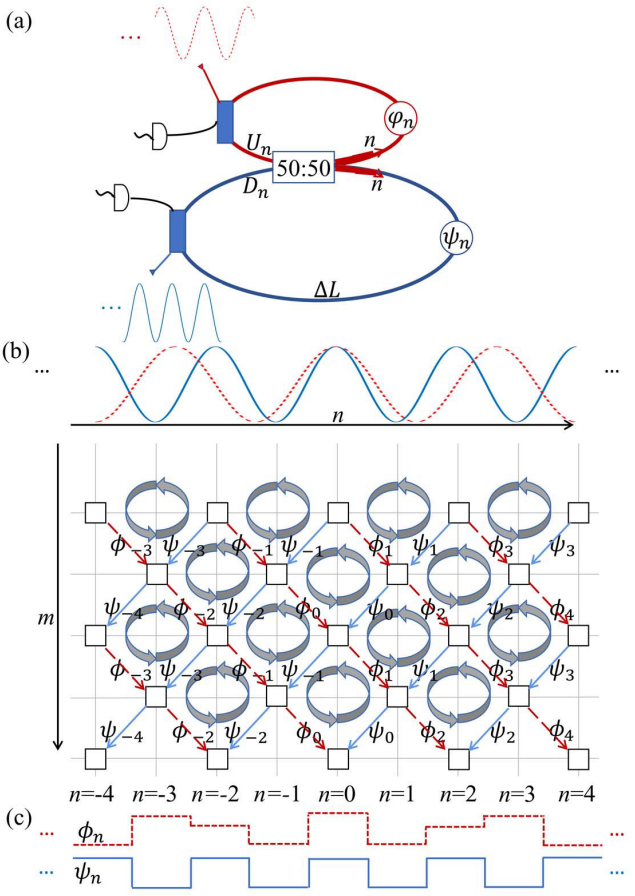

FIG. 1. (a) Schematic of two mutually coupled optical fiber loops with a different length ΔL. (b) The corresponding SPL of the fiber loops mapped onto a $(1 + 1)D$ lattice (the square represents the fiber coupler). (c)The distribution of phase modulation ϕ_n and ψ_n.

treat the evolution of discrete time as a quantum state through the optical grid, which is decomposed into a translation-like operation of free propagation along with directional links and local scattering processes. The output pulses generated after $m + 1$ round trips were

$$\begin{bmatrix} U_{n-1}^{m+1} \\ D_{n+1}^{m+1} \end{bmatrix} = \begin{bmatrix} e^{i\phi_n} & 0 \\ 0 & e^{i\psi_n} \end{bmatrix} \begin{bmatrix} \cos\theta & i\sin\theta \\ i\sin\theta & \cos\theta \end{bmatrix} \begin{bmatrix} U_n^m \\ D_n^m \end{bmatrix}, \quad (1)$$

where U_n^m and D_n^m describe the complex amplitudes of pulses in the short and long loops, respectively. The variables θ denote the coupling coefficients of the coupler with a coupling ratio of 50 : 50. The phases in the two loops are represented by ϕ_n and ψ_n. The above equation can be deduced as an iterative equation

$$\begin{aligned} U_n^{m+1} &= e^{i\phi_n}\left[\cos\theta U_{n+1}^m + i\sin\theta D_{n+1}^m\right], \\ D_n^{m+1} &= e^{i\psi_n}\left[\cos\theta D_{n-1}^m + i\sin\theta U_{n-1}^m\right]. \end{aligned} \quad (2)$$

To control the optical transmission in the SPL, we purposely changed the phase modulation functions ϕ_n and ψ_n acting on the phase modulators in the two fiber loops for subsequent round trips. In this work, the phases ϕ_n and ψ_n are set as cosine functions versus the space axis n, which are

expressed as

$$\phi = \begin{cases} \phi_n = A\cos\left(\frac{2\pi n}{d_1}\right), \\ \psi_n = A\cos\left(\frac{2\pi n}{d_2}\right), \end{cases} \tag{3}$$

where A denotes the amplitude of the phase modulation and d_1 and d_2 represent the periods of phase modulation in the short and long loops, respectively. The model of SPL is illustrated in Fig. 1(b), indicating that the values of both phases at the bottom of the figure are discrete because of the discrete apace axis. Owing to phase modulation, there are phase circumfluences with intensities of $\Phi_n = \phi_n + \psi_{n-1} - \phi_{n+1} - \psi_n$ in every unit surrounded by four couplers. As a result, the intensity difference between adjacent n values is $\Delta\Phi = 2(\phi_{n+1} + \psi_n) - \phi_{n+2} - \psi_{n+1} - \phi_n - \psi_{n-1}$. In the SPL, the phase accumulation Φ_n represents the superimposed result of two phases in the two rings, which is equivalent to the potentials in photonic lattices, paving the way for configuring non-moiré and moiré patterns. When the periods (d_1 and d_2) of the two phases are identical, Φ_n remains in the same period, namely, the non-moiré pattern. Once the periods of the two phases are different, the period of Φ_n is the lowest common multiple (LCM) of d_1 and d_2; thus, the moiré pattern is established. To investigate the optical dynamics of the system, it is necessary to derive the band structure in the momentum space. The band structure or dispersion relationship can be obtained by introducing a plane-wave-like Bloch wave into Eq. (2), which is

$$\begin{bmatrix} U_n^m \\ D_n^m \end{bmatrix} = \begin{bmatrix} U \\ D \end{bmatrix} \exp(ikn + i\beta m), \tag{4}$$

where β is the propagation constant, and k is the transverse wave number. Substitute Eq. (4) into Eq. (2) to obtain the eigenfunction

$$H(\theta, \phi)\begin{bmatrix} U \\ D \end{bmatrix} = \lambda\begin{bmatrix} U \\ D \end{bmatrix}, \tag{5}$$

where eigenvalue $\lambda = e^{i\beta}$ is an intrinsic characteristic of SPL. $H(\theta, \phi)$ denotes the Hamiltonian of the system. which is

$$\begin{bmatrix}
0 & 0 & SK_0 & PK_0 & 0 & & & \cdots & & & 0 \\
0 & & & \cdots & & & 0 & PM_0 & SM_0 & 0 & 0 \\
0 & 0 & 0 & 0 & SK_1 & PK_1 & 0 & & \cdots & & 0 \\
PM_1 & SM_1 & 0 & & & & \cdots & & & & 0 \\
\vdots & \vdots & \vdots & \vdots & \ddots & \vdots & \vdots & \vdots & \vdots & \vdots & \vdots \\
0 & & & & \cdots & & & & 0 & SK_{n-1} & PK_{n-1} \\
0 & & \cdots & & 0 & PM_{n-1} & SM_{n-1} & 0 & 0 & 0 & 0 \\
SK_n & PK_n & 0 & & & & \cdots & & & & 0 \\
0 & & & \cdots & & & 0 & PM_n & SM_n & 0 & 0
\end{bmatrix}, \tag{6}$$

where $S = \cos\theta$, $P = \sin\theta$, $K_n = e^{i(k+\phi_n)}$, and $M_n = e^{i(k+\psi_n)}$ were set to simplify H. The dispersion relation is calculated by solving Eqs. (5) and (6). Under the modulation of the two phases, the dimension of H is defined by the total period of phase modulation, that is, two times the LCM of d_1 and d_2. The dynamic properties of an SPL system can be inferred from the band gap and eigenvalue distributions by calculating the eigenfunction. Note that the calculation becomes more difficult with an increase in the matrix dimensions of Eq. (6). The energy bands cannot be explicitly expressed by equations; only the diagrams are provided in the following sections.

III. RESULTS AND DISCUSSIONS

A. Optical dynamics in non-moiré periodic phase accumulations

First, we consider the non-moiré periodic phase accumulation case, in which the periods of the two phases are coincident. To investigate the optical dynamics, the phase accumulations Φ_n, band structures according to the eigenfunction, and light transmission were investigated by numerically calculating Eq. (2) were adopted. The corresponding results are shown in Fig. 2. The phase accumulations shown in Figs. 2(a1) to 2(a3) were calculated using the expression Φ_n. By changing the phase modulation periods d_1 and d_2, the phase accumulations are distributed periodically, analogous to the potential of the Bragg lattice. This clearly shows that as the period increases, the value of adjacent phase accumulations becomes close, indicating that the band gaps between them are narrow. By calculating the band structure, it was found that the band structure was repeated twice in the first Brillouin zone values $-\pi \sim \pi$. Thus only the band structures from 0 to π are provided for a clearer investigation as there are many bands according to Eq. (6). The band structures are significantly affected by the phase modulation periods, as depicted in Figs. 2(b1) to 2(b3). The band structure with $d_1 = d_2 = 3$ is shown in Fig. 2(b1), which contains three bands with a period of $2\pi/3$ with respect to wave number k. For the condition $d_1 = d_2 = 7$, [see Fig. 2(b2)], the number of bands increases to seven, decreases in the period versus k, and becomes flatter than that in Fig. 2(b1). Similarly, there were 13 energy bands with $d_1 = d_2 = 13$. In this case, three flat bands are observed [Fig. 2(b3)]. From these results, we conclude that the phase modulation period determines the number of energy bands. When the periods of dual-phase modulations are equal ($d_1 = d_2 = d$), the period (d) is identical to the number of bands, and the energy bands become flat.

A series of simulations of the SPL transmission dynamics were performed. A narrow Gaussian beam centered at position n was employed as the initial excitation. Figures 2(c1) to 2(c3) show the simulated results of the optical transmission and accompanying participation ratio $P(m) = (\sum_n |U_n^m|^2)^2 / \sum_n |U_n^m|^4$ to represent the localization intensity

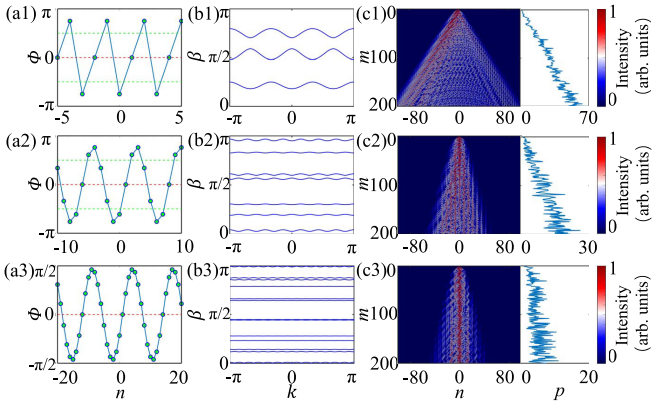

FIG. 2. (a1)–(a3) Phase circumfluence Φ_n, (b1)–(b3) band structures, (c1)–(c3) propagation dynamics and participation ratio for the conditions: top row $d_1 = d_2 = 3$, middle row $d_1 = d_2 = 7$, and bottom row $d_1 = d_2 = 13$, respectively. The red line indicates that the energy is concentrated near the input pulse in (c3). All other elements are initially set to zero except $U_0^0 = 1$ in (c1)–(c3). In the above situations, the variable $A = \pi/2$ remains invariant.

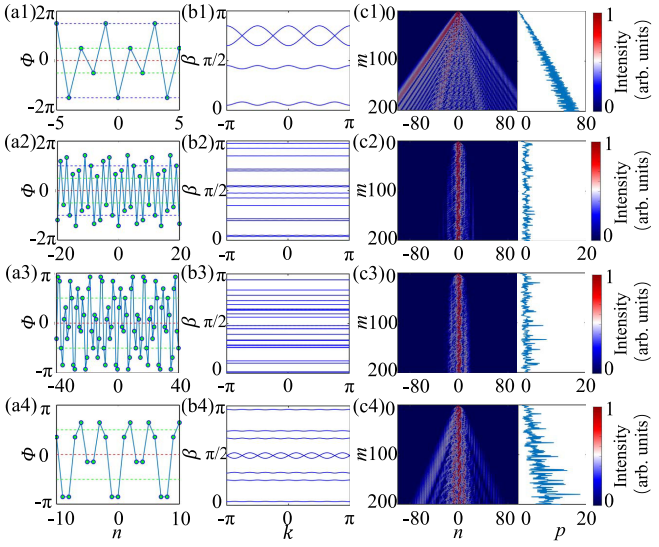

FIG. 3. The same as Fig. 2 for four conditions of top row $d_1 = 2$, $d_2 = 4$; second row $d_1 = 2$, $d_2 = 7$; third row $d_1 = 4$, $d_2 = 7$; and bottom row $d_1 = 4$, $d_2 = 8$, respectively.

[1]. The smaller the value of $P(m)$, the stronger the localized intensity. When the period of the phase modulation is small ($d_1 = d_2 = 3$), a discrete diffraction pattern is obtained, as shown in Fig. 2(c1), the participation ratio increases linearly. As the phase modulation period increases, discrete diffraction is suppressed, as shown in Fig. 2(c2). For $d_1 = d_2 = 13$, energy diffusion is weakened and most of the light is localized near the input site owing to the emergence of flat bands. Correspondingly, the optical pattern exhibited a narrow bright line at the center. The final value of $P(m)$ is less than 10, which also indicates optical localization. The above results show that the optical localization arises with the increase of the phase modulation period and the strong localization attributes to the emergence of flat bands that originate from the weaker coupling between adjacent compound cells as the result of the enlarged modulation period.

B. Optical dynamics in moiré periodic phase accumulations

In the case of moiré periodic phase accumulations, the phase modulation periods in the two loops are different. The phase accumulations as a function of the discrete position n exhibit moiré patterns, as shown in Figs. 3(a1) to 3(a4). There are four and eight energy bands for the cases of $d_1 = 2, d_2 = 4$ and $d_1 = 4, d_2 = 8$, respectively, as shown in Figs. 3(b1) and 3(b4), both of which have degenerate bands that originate from phase accumulation differences of 2π and 0, respectively. No flat bands were observed in the two cases [see Figs. 3(b1) and 3(b4)]. The corresponding transmission behaviors belong to discrete diffraction with different diffraction angles when a narrow Gaussian beam is injected into the short loop at the central position axis. In addition, the linearly growing $P(m)$ verifies discrete diffraction propagation. For comparison, for $d_1 = 2$ and $d_2 = 7$, there were 14 energy bands [Fig. 3(b2)]. The number of bands is the smallest common multiple of d_1 and d_2. Figures 2(b1) to 2(b3) and Figs. 3(b1) to 34b1) show that the number of bands increases and the bands gradually become flat as the value of LCM(d_1, d_2) increases. When d_1 and d_2 are not multiples, the number of energy bands increases and many flat bands are induced. The generation of abundant flat bands is related to the variation of the moiré period, which is different from the specifically designed flat band systems with special symmetry or topological protection [43–47], such as quasi-one-dimensional rhombic lattice and Su-Schrieffer-Heeger model in one dimension. The superiority of abundant flat bands allows flexibility in choosing the incident position, thereby reducing the difficulty of optical localization. It was found that strong optical localization was generated when the participation ratio was less than 10 and the amplitude was small, as illustrated in Figs. 3(c2) and 3(c3), respectively. Therefore, based on the participation ratio, the localization shown in Fig. 3(c2) is stronger than that shown in Fig. 3(c3). Although there are more flat bands in Fig. 3(c3), optical localization is weaker than that in Fig. 3(c2) because the band gap decreases. From the results, the localization intensity is not only dependent on the number of flat bands but is also affected by the band-gap width.

C. Statistics of optical localization area

According to the discussion above, the transition from discrete diffraction to optical localization depends on the number of flat bands. However, the localization intensity cannot be distinguished directly using only the number of flat bands. To qualitatively study the localization intensity in the SPL modulated by the two phases, the inverse participation ratio [48] is used to intuitively investigate the localization. As shown in Fig. 4, the average values of $1/P(m)$ in the last 100 grid points m were calculated with different d_1 and d_2. The color change from blue to red represents a gradually increasing localization intensity. In Fig. 4(a), when the phase modulation periods in the two loops are identical, the localization becomes stronger with an increase in the period, as previously investigated in

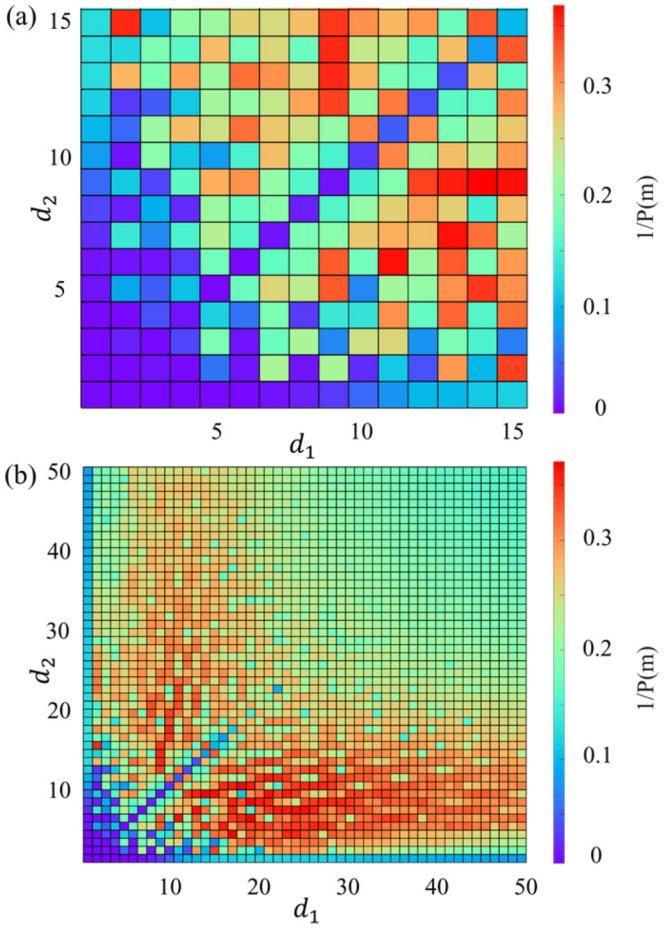

FIG. 4. Statistical diagram of localization intensities versus d_1 and d_2. The intensities correspond to the average value of inverse P in the last 100 grid point m, and the larger the intensity, the stronger the localization. (a,b) are the small- and large-scale periods, respectively.

Sec. III A. One of the two modulation periods is 1, and there is a similar localization principle for the cases of identical phase periods. However, the localization strengths under the above two conditions were very weak. When the phase modulation periods are different, there is no obvious principle for the localization strength; however, the localization pattern is almost symmetric on the main diagonal, which is clearly shown in Fig. 4(b). This is because of the symmetrical positions of d_1 and d_2. This discrepancy arises because of different band excitations by the initial pulse. However, the maximum localization intensity with a participation ratio less than 2.3 is generated in the area of d_1 or d_2 in the range of 3 to 15. In addition, for larger d_1 and d_2, the localization strength becomes weaker. This is reasonable because the energy bands are restricted within $-\pi \sim \pi$, the band gap becomes narrower as the number of bands increases, reducing the difficulty of transitions between energy levels.

D. Optical localization transition in large modulation period of phases

In this section, the band structures and optical dynamics of the SPL with a large phase modulation period are

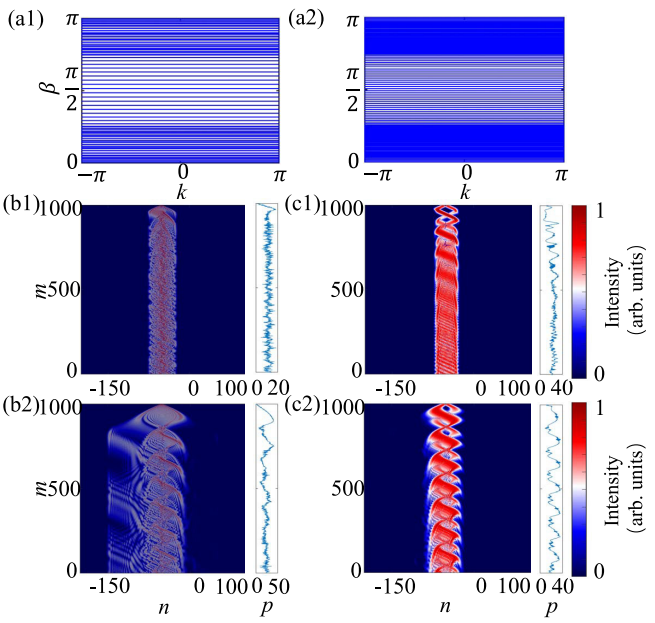

FIG. 5. Optical dynamics in SPL with large periods of phase modulations. Band structures with identical dual-period modulation of (a1) $d_1 = d_2 = 100$, (a2) $d_1 = d_2 = 200$. Pulse behaviors with narrow Gaussian beam excitation (b1) $d_1 = d_2 = 100$, (b2) $d_1 = d_2 = 200$, the narrow beam has a width of $2\delta = 1$ and an initial phase tilt of $k_0 = 0$. Pulse behaviors with wide Gaussian beam excitation (c1) $d_1 = d_2 = 100$, (c2) $d_1 = d_2 = 200$, the wide beam has a width of $2\delta = 12$ and an initial phase tilt of $k_0 = \pi/2$. The initial incident position of the Gaussian beam is $n = -53$.

simulated. Figures 5(a1) and 5(a2) show band structures with periods $d_1 = d_2 = 100$ and $d_1 = d_2 = 200$, respectively. The band-gap widths were narrower than those in the case of small-period phase modulation. In addition, the energy bands present a density distribution and all energy bands are flat. The incidence of a narrow Gaussian beam and a wide Gaussian beam was simulated by the numerical solution of Eq. (2). The dynamic participation ratio is also simulated on the right side of Figs. 5(b1) to 5(b4). The simulation results (numerical value of participation rate) show that the localization intensity decreases with an increase in the modulation period when a narrow Gaussian beam is incident, which coincides with the statistical principle. If a wider Gaussian beam is incident, the light is first split into two oscillating pulses, which is caused by alternately exciting the two density regions of the energy bands. Finally, the light becomes localized in a region owing to its small dispersion. The localization region is broadened by comparing it with the case $d_1 = d_2 = 100$. Furthermore, by altering the wave number k, long-range optical vibration with an oscillation period of ∼143 was formed. The narrower the incident Gaussian beam, the greater the number of excited energy bands, resulting in a weaker localization intensity. Under long-period phase modulation, light can be transferred from vibration to localization by altering the incident position site n and wave number k.

IV. EXPERIMENTAL PROPOSAL

To prove the feasibility of our study, a corresponding experimental arrangement is suggested according to the

theoretical model (Fig. 1). A 50/50 optocoupler (OC) connects two fiber loops with an average length of 4 km, with a lower ring dozens of meters longer than the other [36,39,49,50]. Each loop has an erbium-doped fiber amplifier (EDFA) to compensate for the optical loss of various components. Phase modulators (PMs) were inserted into each loop to obtain the phases of this study. Zero dispersion is guaranteed by inserting two dispersion compensation fibers (DCF) into the loops, and an isolator (ISO) is used to ensure that the pulse propagates unidirectionally. Polarization beam splitters (PBS) and polarization controllers (PCs) are used to manage the polarization state in the birefringence of fibers and EDFAs to obtain good optical interference. The phase accumulation generated by two-phase modulators was previously realized in Ref. [39]. Therefore, it is simple to obtain phase accumulation based on our theoretical model by adding two PMs controlled by a discrete cosine function to the two loops.

V. CONCLUSION

In conclusion, we study the optical localization transition in SPL with two-phase modulators in two fiber loops. By altering the periods of both phases, the number of energy bands is defined by the LCM of d_1, d_2, and there is a localization-delocalization transition in the small-period region. From the statistical diagram of inverse participation ratios, strong localization is distributed symmetrically on the diagonal line and concentrates in the region of $3 < d_1 < 15$ or $3 < d_2 < 15$. In the large modulation period area, the localization intensities are weakened owing to the narrower band gap. Therefore, we further investigated the band structures and optical transmission in SPL with large modulation periods. The energy bands exhibited a density distribution and there was a transition from optical vibration to localization by changing both the position and wave number of the input Gaussian wave packet. This study explores the effects of moiré modulation and non-moiré modulation on pulse dynamics in an SPL system, the transmission trajectory of which is deterministic and repeatable, which provides an alternative way to achieve optical localization in discrete fiber synthetic dimension systems.

ACKNOWLEDGMENTS

This work was supported by the National Key Research and Development Project of China (Grant No. 2019YFA0705000), National Natural Science Foundation of China (NSFC) (Grants No. 12104272, No. 12192254, No. 91750201, and No. 11974218), Innovation Group of Jinan (Grant No. 2018GXRC010), Local Science and Technology Development Project of the Central Government (Grant No. YDZX20203700001766).

[1] A. V. Pankov, I. D. Vatnik, D. V. Churkin, and S. A. Derevyanko, Opt. Express **27**, 4424 (2019).
[2] C. Huang, C. Shang, J. Li, L. Dong, and F. Ye, Opt. Express **27**, 6259 (2019).
[3] X. Mao, Z. Shao, H. Luan, S. Wang, and R. Ma, Nat. Nanotechnol. **16**, 1099 (2021).
[4] K. J. Vahala, Nature (London) **424**, 839 (2003).
[5] R. M. Ma and R. F. Oulton, Nat. Nanotechnol. **14**, 12 (2019).
[6] S. Longhi, Phys. Rev. B **80**, 235102 (2009).
[7] J. Zeng, Y. Hu, X. Zhang, S. Fu, H. Yin, Z. Li, and Z. Chen, Opt. Express **29**, 25388 (2021).
[8] D. M. Jović, Y. S. Kivshar, C. Denz, and M. R. Belić, Phys. Rev. A **83**, 033813 (2011).
[9] T. Schwartz, G. Bartal, S. Fishman, and M. Segev, Nature (London) **446**, 52 (2007).
[10] Y. Lahini, A. Avidan, F. Pozzi, M. Sorel, R. Morandotti, D. N. Christodoulides, and Y. Silberberg, Phys. Rev. Lett. **100**, 013906 (2008).
[11] S. Xia, D. Jukić, N. Wang, D. Smirnova, L. Smirnov, L. Tang, D. Song, A. Szameit, D. Leykam, J. Xu, Z. Chen, and H. Buljan, Light Sci. Appl. **9**, 147 (2020).
[12] F. Fedele, J. Yang, and Z. Chen, Opt. Lett. **30**, 1506 (2005).
[13] I. Makasyuk, Z. Chen, and J. Yang, Phys. Rev. Lett. **96**, 223903 (2006).
[14] J. Wang, J. Yang, and Z. Chen, Phys. Rev. A **76**, 013828 (2007).
[15] C. Sheng, Y. Wang, Y. Chang, H. Wang, Y. Lu, Y. Yang, S. Zhu, X. Jin, and H. Liu, Light Sci. Appl. **11**, 243 (2022).
[16] D. H. Dunlap and V. M. Kenkre, Phys. Rev. B **34**, 3625 (1986).
[17] L. J. Maczewsky, K. Wang, A. A. Dovgiy, A. E. Miroshnichenko, A. Moroz, M. Ehrhardt, M. Heinrich, D. N. Christodoulides, A. Szameit, and A. A. Sukhorukov, Nat. Photonics **14**, 76 (2020).
[18] P. Wang, Y. Zheng, X. Chen, C. Huang, Y. V. Kartashov, L. Torner, V. V. Konotop, and F. Ye, Nature (London) **577**, 42 (2020).
[19] C. Huang, F. Ye, X. Chen, Y. V. Kartashov, V. V. Konotop, and L. Torner, Sci. Rep. **6**, 32546 (2016).
[20] Q. Fu, P. Wang, C. Huang, Y. V. Kartashov, L. Torner, V. V. Konotop, and F. Ye, Nat. Photonics **14**, 663 (2020).
[21] R. Xue, W. Wang, L. Wang, H. Chen, R. Guo, and J. Chen, Opt. Express **25**, 5788 (2017).
[22] M. H. Naik and M. Jain, Phys. Rev. Lett. **121**, 266401 (2018).
[23] K. Dong, T. Zhang, J. Li, Q. Wang, F. Yang, Y. Rho, D. Wang, C. P. Grigoropoulos, J. Wu, and J. Yao, Phys. Rev. Lett. **126**, 223601 (2021).
[24] D. Kang, Z. Zuo, Z. Wang, and W. Ju, Appl. Phys. Lett. **119**, 061602 (2021).
[25] Y. V. Kartashov, F. Ye, V. V. Konotop, and L. Torner, Phys. Rev. Lett. **127**, 163902 (2021).
[26] Y.-R. Zhang, Z.-Z. Zhang, J.-Q. Yuan, M. Kang, and J. Chen, Front. Phys. **14**, 53603 (2019).
[27] L. Yuan, Q. Lin, M. Xiao, and S. Fan, Optica **5**, 1396 (2018).
[28] T. Ozawa, H. M. Price, N. Goldman, O. Zilberberg, and I. Carusotto, Phys. Rev. A **93**, 043827 (2016).
[29] A. Regensburger, C. Bersch, M.-A. Miri, G. Onishchukov, D. N. Christodoulides, and U. Peschel, Nature (London) **488**, 167 (2012).
[30] L. Yuan, Y. Shi, and S. Fan, Opt. Lett. **41**, 741 (2016).
[31] K. Kikuchi, J. Lightwave Technol. **34**, 157 (2015).

[32] I. S. Amiri, M. R. K. Soltanian, and H. Ahmad, *Optical Communication Systems: Fundamentals, Techniques and Applications* (Nova Science Publishers, Inc., NY, 2015), Chap. 2.
[33] P. Kok and B. W. Lovett, *Introduction to Optical Quantum Information Processing* (Cambridge University Press, Cambridge, England, 2010).
[34] I. D. Vatnik, A. Tikan, G. Onishchukov, D. V. Churkin, and A. A. Sukhorukov, Sci. Rep. **7**, 4301 (2017).
[35] M. Wimmer and U. Peschel, Sci. Rep. **8**, 2125 (2018).
[36] M. Wimmer, A. Regensburger, C. Bersch, M.-A. Miri, S. Batz, G. Onishchukov, D. N. Christodoulides, and U. Peschel, Nat. Phys. **9**, 780 (2013).
[37] M. Wimmer, M.-A. Miri, D. Christodoulides, and U. Peschel, Sci. Rep. **5**, 17760 (2015).
[38] A. Regensburger, M.-A. Miri, C. Bersch, J. Näger, G. Onishchukov, D. N. Christodoulides, and U. Peschel, Phys. Rev. Lett. **110**, 223902 (2013).
[39] A. V. Pankov, I. D. Vatnik, D. V. Churkin, and A. A. Sukhorukov, Sci. Rep. **9**, 3464 (2019).
[40] S. Weidemann, M. Kremer, T. Helbig, T. Hofmann, A. Stegmaier, M. Greiter, R. Thomale, and A. Szameit, Science **368**, 311 (2020).
[41] S. Weidemann, M. Kremer, S. Longhi, and A. Szameit, Nat. Photonics **15**, 576 (2021).
[42] S. Weidemann, M. Kremer, S. Longhi, and A. Szameit, Nature (London) **601**, 354 (2022).
[43] S. Mukherjee and R. R. Thomson, Opt. Lett. **40**, 5443 (2015).
[44] S. Mukherjee, A. Spracklen, D. Choudhury, N. Goldman, P. Öhberg, E. Andersson, and R. R. Thomson, Phys. Rev. Lett. **114**, 245504 (2015).
[45] N. Masumoto, N. Y. Kim, T. Byrnes, K. Kusudo, A. Löffler, S. Höfling, A. Forchel, and Y. Yamamoto, New J. Phys. **14**, 065002 (2012).
[46] W. Yan, H. Zhong, D. Song, Y. Zhang, S. Xia, L. Tang, D. Leykam, and Z. Chen, Adv. Opt. Mater. **8**, 1902174 (2020).
[47] H. Ma, Z. Zhang, P.-H. Fu, J. Wu, and X.-L. Yu, Phys. Rev. B **106**, 245109 (2022).
[48] D. J. Thouless, Phys. Rep. **13**, 93 (1974).
[49] M. Wimmer, H. M. Price, I. Carusotto, and U. Peschel, Nat. Phys. **13**, 545 (2017).
[50] Z. Wen, B. Lu, K. Wang, X. Qi, and J. Bai, J. Opt. Soc. Am. B **37**, 3152 (2020).